The Influence of Microphysics in the Formation of Intense Wake Lows: A Numerical Modeling Study

WILLIAM A. GALLUS JR.*

Department of Atmospheric Science, Colorado State University, Fort Collins, Colorado

(Manuscript received 6 July 1995, in final form 4 April 1996)

ABSTRACT

A two-dimensional cloud model is used to investigate whether microphysical processes alone within the stratiform rain regions of mesoscale convection systems can induce strong descent and intense surface wake lows accompanying such systems. Idealized simulations are run with a domain that captures the back edge of the stratiform rain region. A simplified microphysical field, representing snow alone, is prescribed within the stratiform cloud to produce radar reflectivities similar to observations. When the prescribed snow field is assumed time-independent, strong subsidence develops but does not induce an intense wake low since microphysical cooling strongly opposes adiabatic warming. Simply increasing snow quantities, although resulting in heavier rain rates and stronger subsidence, does not produce significant pressure falls. However, when precipitation rates are prescribed to decrease with time as might occur with collapsing precipitation cores, subsidence induces greater pressure falls, and a tighter pressure gradient near the wake low, in better agreement with observations.

1. Introduction

Within the stratiform rain region of squall lines a three-tiered flow structure often exists including an ascending front-to-rear (FTR) jet at middle and high levels, a descending rear-to-front (RTF) current called the rear-inflow jet at a somewhat lower altitude, and a low-level FTR jet near the surface (Smull and Houze 1987). In most cases, the rear-inflow jet descends rather gradually, approaching the surface near the convective line region (e.g., Johnson and Hamilton 1988). This descending jet is believed to play a role both in the formation of a surface mesohigh just behind the leading convective line (Fovell and Ogura 1989) and a wake low that generally lies near or just behind the back edge of surface precipitation (Zhang and Gao 1989). It has been proposed that this region of lower pressure develops when the adiabatic warming of descent is not balanced by the diabatic cooling from evaporation and sublimation (Johnson and Hamilton 1988). Several studies have noted that the wake low reaches its maximum intensity during the dissipating stage of an MCS (Williams 1963; Johnson and Hamilton 1988).

In some mesoscale convective systems (MCS)s, however, the gradual descent of the rear-inflow jet is interrupted by a narrow zone in which strong subsidence occurs. In the 3–4 and 23–24 June 1985 PRESTORM cases, the rear-inflow jet descended at a rate of 6 m s^{-1} in a narrow zone near the back edge of the surface precipitation (Stumpf et al. 1991; Johnson and Bartels 1992). The jet appeared to be blocked. Associated with this intense descent in the 3–4 June system was a deep surface wake low with pressure gradients as large as 2 mb over a 5-km distance, and pressure falls at individual sites of 6 mb in a 30-min period (Stumpf et al. 1991). In the 3–4 June system, the intense wake low occurred just behind the most intense reflectivity in the stratiform region (Stumpf et al. 1991). In addition, the southern portion of the MCS, which was not trailed by significant stratiform precipitation, lacked a wake low, suggesting that processes within the stratiform region are important to its formation. A somewhat similar distribution of pressure, including an intense wake low associated with an 8 mb pressure drop in 10 min, occurred in an asymmetric MCS on 28 May 1995 (Scott and Rutledge 1995). Pressure falls of 9 mb within 20 min have also been observed at the rear edge of the stratiform region in some squall lines (Williams 1954; Bosart and Seimon 1988).

Some wake lows have also been associated with sudden intense temperature rises known as heat bursts (Johnson et al. 1989; Bernstein and Johnson 1994). The same lower-atmospheric temperature and stability conditions that occur with wake lows may be favorable for heat bursts when a shallow stable layer exists near

* Current affiliation: Dept. of Geological and Atmospheric Science, Iowa State University, Ames, Iowa.

Corresponding author address: Dr. William A. Gallus Jr., Department of Geological and Atmospheric Sciences, Iowa State University, 3010 Agronomy Hall, Ames, IA 50011.
E-mail: wgallus@synoptic.agron.iastate.edu

the surface. In the 23–24 June 1985 case, strong descent near the rear edge of a strong reflectivity gradient and a wake low at the back of the stratiform region deformed a surface stable layer with resulting dramatic warming and drying at the surface (Bernstein and Johnson 1994).

Large domain mesoscale models have reasonably simulated wake lows of moderate intensity associated with tropical oceanic (e.g., Nicholls 1987) and continental convection (e.g., Lafore and Moncrieff 1989; Caniaux et al. 1995) and midlatitude convection (e.g., Zhang et al. 1989). The pressure minima generally occur behind the main region of stratiform precipitation in areas of subsidence and lower tropospheric warming. In these large domain simulations, processes outside the convective systems may contribute to the warming and pressure falls. Large pressure falls with intense wake lows like that occurring in the 3–4 June system, however, have not been successfully simulated at this time.

In Gallus and Johnson (1995a,b; hereafter GJa, GJb), a two-dimensional cloud model with a detailed bulk microphysical parameterization was developed to investigate the stratiform region of the 10–11 June PRE-STORM squall line case, a classic example of a squall line with a trailing stratiform rain region and a gradually descending rear-inflow jet. Although the domain size was limited and the convective line not explicitly modeled but instead represented by prescribed convective line inputs that drove the simulation, the model reproduced observed stratiform region features rather well, and showed that stratiform circulations were somewhat dependent upon the amount of hydrometeors advected rearward from the convective line region, and also the environmental stability. The rear-inflow jet descended gradually in the simulations. In spite of a well-developed mesoscale downdraft, the intensity of the surface wake low was underestimated by the model, which used a 5-km horizontal resolution. The weakness of the wake low may have been due to a lack of strong rear-inflow extending above the melting level. Without an opposing current of dry air, sufficient water vapor advected rearward to minimize the amount of sublimation in this region. Stensrud et al. (1991) found in a 1D modeling study that sublimational cooling could be large and along with other forms of microphysical cooling could initiate a strong downdraft near the rear of stratiform regions.

The deficiency of the small domain Gallus and Johnson model to produce a significant wake low in the 10–11 June simulations may cast doubt on the idea that microphysical processes alone can force a downdraft as strong as several meters per second and induce an intense surface wake low, especially one as strong as those observed in both the 3–4 June and 23–24 June PRE-STORM MCSs (e.g., Stumpf et al. 1991; Johnson and Bartels 1992). However, microphysical processes are known to be important in this region, with Zhang and Gao (1989) finding a strong rear-inflow absent without appropriate microphysics, and the 1D model of Stensrud et al. (1991) showing that a 3.9 m s^{-1} downdraft could form from microphysics alone. The GJa and GJb results suggest that it may be difficult for microphysical cooling to induce sufficient descent so that adiabatic warming exceeds the cooling and results in significant pressure falls at the surface. Schmidt and Cotton (1990) have proposed that interacting gravity wave circulations produced when upper-level flow is blocked by the convectively induced mesohigh contribute to the initial descent of the rear-inflow jet at high levels. This interaction may also contribute to the formation of the wake low rearward of the main precipitation area. Successful simulation of such an interaction would be highly dependent upon a model's ability to appropriately simulate the environmental winds and stability near the rear of the system.

In this paper the 2D cloud model used in GJa and GJb is applied to the rearmost portion of a stratiform region, at a time when the stratiform region is well developed. The primary emphasis of the paper is on the effect of microphysical cooling on the wake low, via the downdrafts produced. This work is somewhat analogous to the 1D modeling study of Stensrud et al. (1991), which used a similar microphysical scheme (Lin et al. 1983; Ziegler 1985). However, the emphasis in that work was on the mesoscale downdraft and its effects on the wind field, with less discussion of any influence on the surface pressure field.

Two different highly idealized simulations are run to study the 3–4 June PRE-STORM case in which the circulation behaved rather differently from the 10–11 June system. The two simulations use a 2-km horizontal resolution to better resolve the intense circulations that occurred in that stratiform region. Although the 3–4 June PRE-STORM system was not highly two-dimensional like the 10–11 June case, the small domain size, 128 km, applied to only the rearmost portion of the stratiform region in the vicinity of the strongest subsidence should prevent the 2D restriction from introducing serious errors. For simplicity in the idealized experiments, all of the frozen hydrometeors are assumed to be represented in the snow field prescribed in the simulations above the melting level, and the effects of ice or graupel are neglected. In one simulation, the snow field prescribed in the anvil cloud is time-independent, and rain rates do not decrease. With the prescribed ambient wind shear, this precipitation field would typify a steady or expanding stratiform region.

In another simulation the snow field is prescribed to decrease markedly so that rain rates also decrease with time, representing crudely either a rapidly moving stratiform region, or a system in which collapsing precipitation cores play a role. A rapidly intensifying wake low in the 23–24 June PRE-STORM system was associated with an equally rapid dissipation of the stratiform rain region. Johnson et al. (1989) have suggested

that the dissipation acts as a collapsing cold pool or spreading density current, which has been shown in modeling studies (Miller and Betts 1977; Thorpe et al. 1980) to result in warming atop the spreading density current. In this simulation where the rain rates decrease, a more intense wake low is produced, more closely resembling observations.

The two idealized simulations may appear overly simplified, as it can be argued that rapid dissipation of the stratiform precipitation must be caused by either the demise of the convective line, which seeds it, or a change in the wind shear, which cuts off trajectories from the convective region. Neither of these processes are simulated in this model. Simulations of the 10–11 June system with this model (GJa, GJb) failed to produce rear inflow as strong or as high into the atmosphere at the rear of the system as was observed. Without this strong opposing flow to the front-to-rear jet exiting the convective line, too much vapor advected rearward and microphysical processes and the dynamic response to them were adversely affected in this region. Thus, even high-resolution simulations based on initial data from the mature stage of the simulated 10–11 June system fail to depict a realistic wake low.

Therefore, the best way to take advantage of the detailed microphysical scheme in this model, and to investigate the role of microphysics in the formation and evolution of wake lows is to initialize the model with conditions that have been observed in well-established stratiform regions around the time that wake lows have developed. Rapid demise of precipitation cores in the stratiform region was not simulated in GJa and GJb, when convective inputs decreased at a rate determined by observations. However, a rapid decrease of reflectivity intensities has been observed in some systems (e.g., Johnson et al. 1989). Perhaps enhanced convective-like precipitation features may be caused by interaction of the stratiform circulation with certain environmental wind regimes. Because this model is unable to simulate the development of such features with its simplified initialization, the rapid decrease in precipitation intensity is prescribed in the appropriate simulation. It is assumed that more complicated interactions have taken place to produce the initial core of precipitation and to lead to its rapid weakening.

2. Description of the numerical model and initialization technique

The 2D cloud model used for the wake-low simulations is based on the deep anelastic equations of Ogura and Phillips (1962) with incorporation of the six-water-class bulk microphysical scheme of Rutledge and Hobbs (1983, 1984). For simplicity, radiative effects are excluded, the Coriolis force is neglected and flat terrain is used. Details of the basic model equations and important numerical aspects are discussed in GJa. For the simulations discussed in this paper, a 2-km horizontal resolution is used over a 128-km domain. A 300-m vertical resolution is used with a model top just below the tropopause, at 12.5 km. A time step of 10 s is used in these simulations, and the model is integrated for 110 min.

With the exception of the wind field, the model design and initialization of winds are similar to that used by Szeto et al. (1988) to study the effects of melting and evaporation on stratiform region circulations. The purpose of this study is to investigate the degree to which microphysical cooling can affect the surface pressure field through the creation of downward motion in a limited area near the rear of the stratiform region. To simplify the simulations, initial conditions are chosen to represent a mature stratiform region where shear exists between midlevel and upper-level flow. The evolution of a stratiform region was discussed in GJa and GJb. It is acknowledged that the dynamics and structure of the anvil cloud itself would also be evolving during this time and this evolution is restricted in this study with the rigid prescription of snow content in the cloud. However, the wake low is generally believed to be hydrostatically induced (Johnson and Hamilton 1988; Stumpf et al. 1991) and primarily the result of low-level warming. Upper-level features not explicitly simulated in this study should have relatively little influence on the wake low itself.

The temperature, moisture, and wind profile used for initialization of the domain is shown in Fig. 1. These fields are assumed to be horizontally homogeneous. The initialization of the temperature and humidity fields is based on the Russell soundings shown in Stumpf et al. (1991) for the 3–4 June MCS at 0000

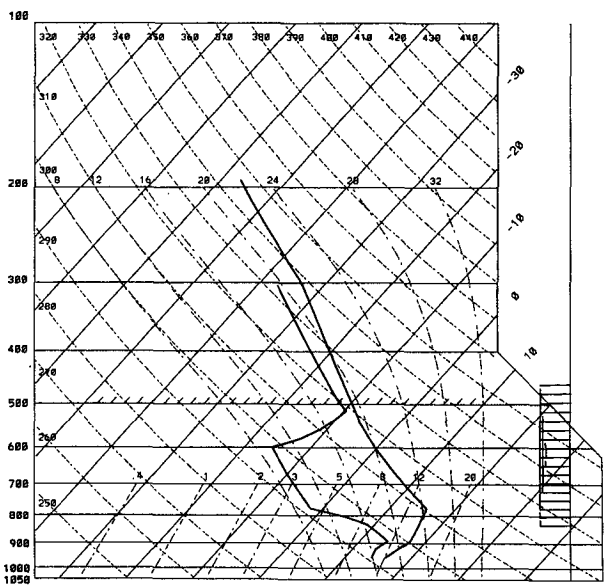

FIG. 1. Initial thermodynamic diagram used for both simulations S1 and S2. Relative winds are shown at the right.

and 0130 UTC. Some modifications are made based upon other soundings that occurred near the back of the stratiform rain regions of both the 10–11 June and 3–4 June system. The appropriate initialization should include temperature and moisture profiles that would be found in a mature stratiform region just prior to the formation of an intense wake low. Because of the small-scale and transient nature of wake lows, such soundings are difficult to obtain. The conditions shown in Fig. 1 may not necessarily occur prior to the formation of all intense wake lows, although for the 3–4 June case, the conditions are supported by the Russell soundings.

The ambient wind in the simulations is simplified by assuming no horizontal velocity except in the 2–7-km layer where RTF flow existed. A rear-inflow jet is assigned a peak magnitude of around 15 m s^{-1} at the melting level, around 4 km. RTF flow was observed over a deep layer in this case (Stumpf et al. 1991). The layer of RTF flow can be seen in the winds plotted at the right of the diagram (Fig. 1). A low-level temperature inversion exists in the lowest 1 km. Relative humidities with respect to water fall from around 80% at the surface to 30% in a dry layer that coincides with the lowest one-half of the rear-inflow zone. Nearly water-saturated conditions occur above 5 km in the anvil cloud. The lapse rates are nearly moist adiabatic from the melting level upward, and rather unstable in the 2 km below the melting level.

The shear initialized within the anvil cloud roughly agrees with observations of the 3–4 June system. The simplified wind profile itself may be thought of as that obtained with a reference frame moving at the same speed as the FTR flow at middle and high levels in the anvil cloud. Therefore, the simulation with a constant snow field would typify an expanding stratiform region, whereas the simulation with rapidly decreasing precipitation rates would more closely resemble a mature or decaying system. In fact, the rapidity of the prescribed decrease of precipitation in S2 could be thought of as representing a collapsing precipitation core, similar to those observed in the 23–24 June system, or a case where an intense reflectivity gradient exists at the rear of a moving stratiform region, as in the 3–4 June case.

Snow is initially prescribed in the rightmost 100 km of the domain at levels above approximately 5 km (Fig. 2). The peak snow mixing ratios are around 3.3 g kg^{-1}, and the snow field is prescribed to be somewhat less away from the rear of the system as implied in observations of the reflectivity field for this case (Stumpf et al. 1991). The snow contents are significantly greater than those used in a 1D study of the 24 June PRESTORM case (Stensrud et al. 1991), and also somewhat greater than those found in simulations of the 10–11 June system with this model (GJa). However, this snow profile creates a reflectivity field agreeing relatively well with observations from the 3–4 June case.

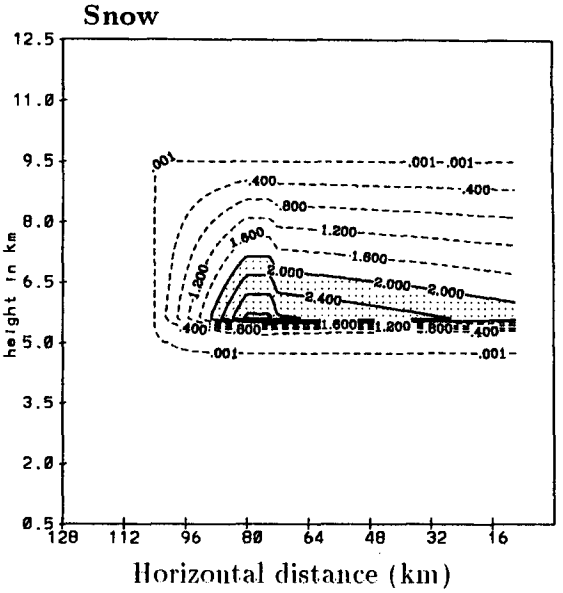

FIG. 2. Initial snow mixing ratios for both simulations. Contour interval is 0.4 g kg^{-1}.

The total snow content is similar to the combined snow and graupel contents assumed for the back of the convective line region in a kinematic study of a GATE squall line (Rutledge 1986). It should again be noted that such mixing ratio data is sparse in the stratiform regions of MCSs, and the wake lows in other systems may occur with smaller quantities under different large-scale conditions. Peak low-level values (around 2–3 km) of model-derived reflectivity reach 40 dBZ in a small region. Stumpf et al. (1991) observe reflectivities near the rear of the stratiform region in the 35–43-dBZ range during the period when the wake low first strengthened to maximum intensity, around 0100 UTC 4 June.

The idealized initialization of the model and the small domain restrict the mechanisms that influence dynamics in the rear of the stratiform region. This limitation of the model may complicate interpretation of results, and prevent realistic simulation of intense wake lows. However, the bulk microphysical scheme is detailed, allowing 23 different interactions between water substance terms, and the scheme has been used successfully not only in the 10–11 June simulations of GJa and GJb, but also in the kinematic studies of Rutledge (1986) and Rutledge and Houze (1987), among others. Therefore, this idealized model should provide some insight into the role that microphysics alone play in the evolution of intense wake lows.

3. Simulation with constant snow field

In the first simulation to be discussed (S1), peak snow mixing ratios above 5.5 km in the anvil cloud are

prescribed to remain constant during the simulation. With the wind profile used in the simulations, the constant snow field in this simulation, in a domain roughly stationary with respect to the ground, implies a system with a rearward-expanding stratiform region.

The rain rates produced by the melting of this snow at 45, 60, and 75 min are shown in Fig. 3. Rainfall reaches the surface after 30 min, and the enhanced snowfall at the rear of the anvil cloud leads to rates exceeding 4 mm h^{-1} by 45 min (Fig. 3a). Rain rates near the melting level increase to 20 mm h^{-1} or greater at 60 and 75 min (Figs. 3b,c). Peak surface rainfall rates exceed 8 mm h^{-1} by 75 min (Fig. 3c). At later times in the simulation, the peak rain rates do not change significantly. Elsewhere in the area beneath the snow field, rainfall is much lighter throughout the simulation. The heaviest surface rainfall occurs in the region around $x = 65$ km.

The sublimation that occurs when the snow falls into the strongly subsaturated air, along with melting and the evaporation of rain, produces a strong downdraft, which is most pronounced near the region of heaviest rainfall. Sublimational cooling rates (not shown) are as large as 7°–8°C h^{-1}, with peak evaporative cooling rates generally reaching 14°–17°C h^{-1}. Melting-induced cooling in the region of heaviest precipitation is as large as 5°–6°C h^{-1}, which is at the upper end of the values given in Leary and Houze (1979) for strat-

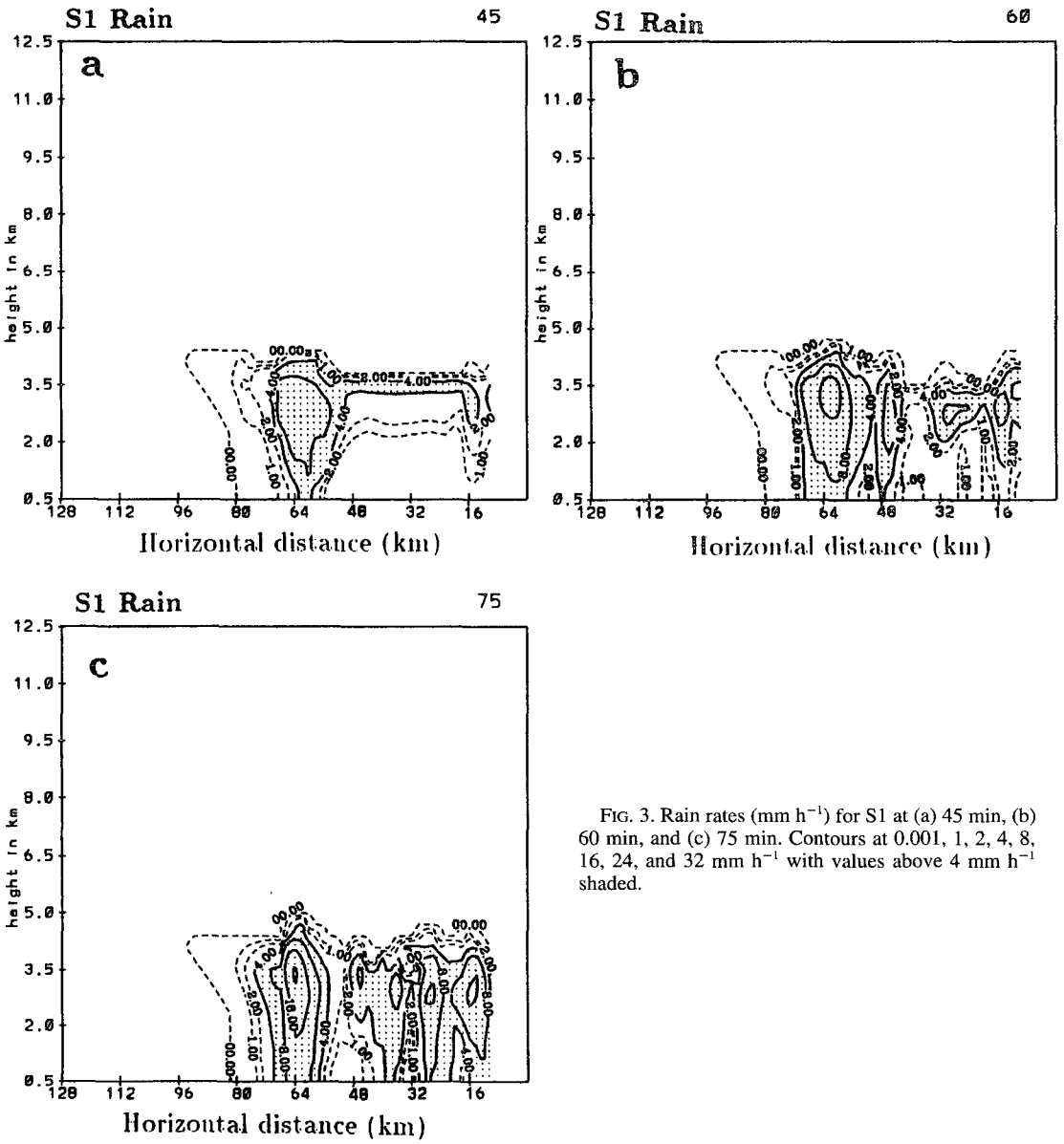

FIG. 3. Rain rates (mm h^{-1}) for S1 at (a) 45 min, (b) 60 min, and (c) 75 min. Contours at 0.001, 1, 2, 4, 8, 16, 24, and 32 mm h^{-1} with values above 4 mm h^{-1} shaded.

iform regions. By comparison, Braun and Houze (1995), and Willis and Heymsfield (1989) found melting-induced cooling rates of 2°–3°C h^{-1} in the 10–11 June PRE-STORM system stratiform region. Similar microphysical cooling rates have been estimated by Smull and Houze (1987) and Stensrud et al. (1991).

Downward motion intensifies rapidly and occurs in a well-defined band at 60 and 75 min (Figs. 4a,b). The maximum downdraft velocity is around 1.6 m s^{-1} at both times. The most intense descent occurs in two regions, one around 4 km, or just below the melting level, in the vicinity of the heaviest surface rainfall, and another at around the 2.5- or 3.0-km level farther from the rear of the stratiform region. Enhanced descent extends rearward from this region along an axis that reaches as high as 7–8 km. The higher level maxima agrees reasonably well with that found by Doppler radar in this case (Stumpf et al. 1991), although the model maxima may be 0.5 km above the level of the observed maxima. The peak descent is not as strong as was observed. This is somewhat surprising since the microphysical cooling agrees with figures estimated in other studies. However, it is possible that the microphysical cooling in this case with its enhanced reflectivities and "blocked" rear-inflow jet was even greater than what the model simulates. In addition, model deficiencies such as coarseness of the horizontal resolution, overly simplified initialization, and lack of realistic evolution of features in the anvil cloud may account for the weakness of the downdraft. Nicholls and Weissbluth (1988) found that 2D simulations of squall lines produced weaker vertical motions than 3D simulations. They suggested that the weaker mesoscale downdraft in a 2D simulation might be attributed to the inability of the cold pool to spread out as well as it would in a 3D simulation.

Strong perturbation horizontal flows develop in the simulation (Fig. 5). The existing RTF flow is intensified in a band that descends from high levels at the rear of the domain to around 3 km in the region of heaviest precipitation. Perturbations exceed 8 m s^{-1} at 60 min (Fig. 5a) and 14 m s^{-1} at 75 min (Fig. 5b). The intense microphysical cooling that occurs when rear inflow of dry air meets significant amounts of snow in the stratiform anvil cloud encourages RTF flow to develop at higher levels than existed initially. Strong convergence is induced just above the melting layer as air rushes into the region of heavy precipitation to compensate for the strong subsidence. Near the surface, FTR flow strengthens to nearly 10 m s^{-1} behind the rain region, helping to spread cool air rearward from the system. Strong convergence (roughly 15 m s^{-1} change over 15 km) around $x = 48$ at both 60 and 75 min (Figs. 5a,b) is similar to that occurring with the "blocked" rear-inflow jet during the 4 June case (Stumpf et al. 1991). The convergence can also be be seen in the total wind field (ambient + perturbation; Fig. 6). Although a complete reversal from RTF to FTR flow is not depicted in this field, it must be noted that the ambient wind profile was chosen relative to the flow in the anvil cloud (so that the prescribed snow initially would experience no horizontal advection). Storm-relative flow in the domain could be estimated by subtracting an average storm-relative flow from all points for the anvil region of this case. The storm-relative flow field would most likely show a rear-inflow jet that appeared to be

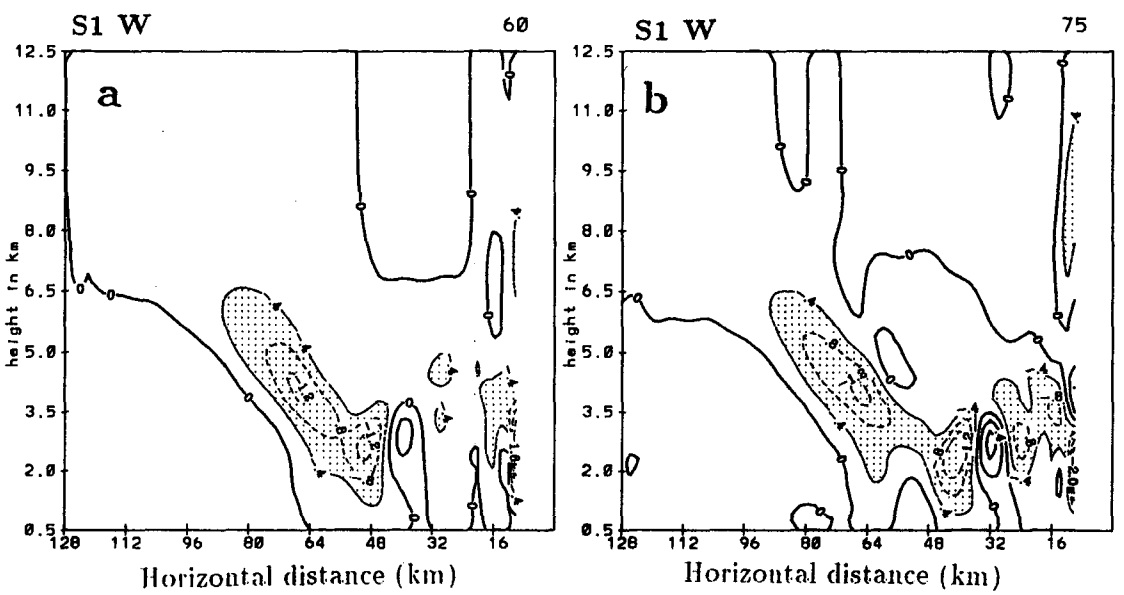

FIG. 4. Vertical velocity (m s^{-1}) at (a) 60 and (b) 75 min, with contour interval of 0.4 m s^{-1}. Values of descent larger than 0.4 m s^{-1} are shaded.

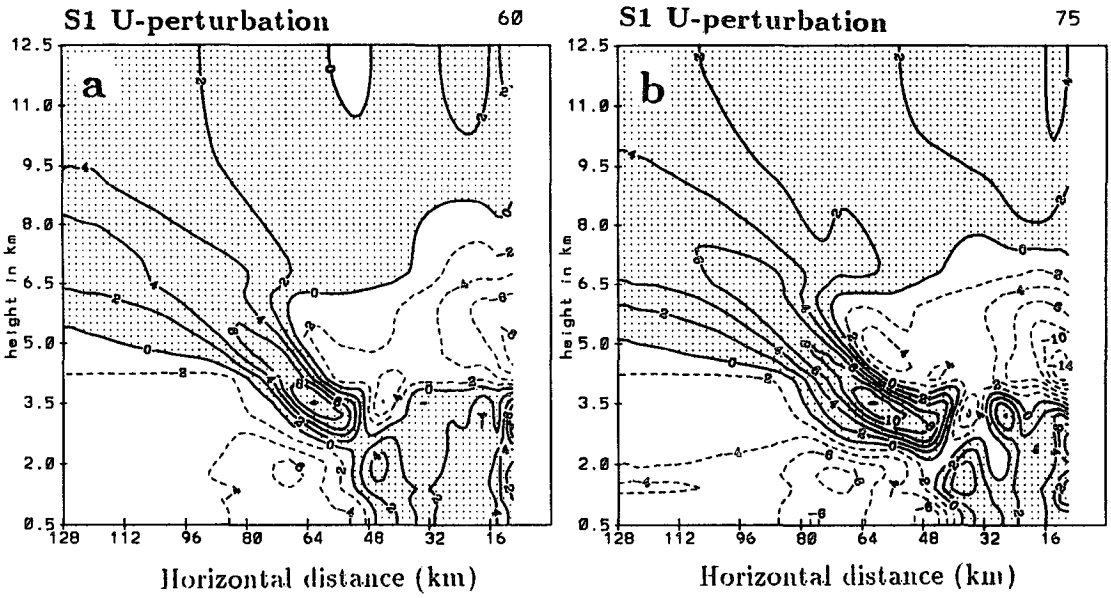

FIG. 5. The U perturbation velocities (m s^{-1}) for S1 at (a) 60 and (b) 75 min, with contour interval of 2 m s^{-1} for magnitudes of 10 m s^{-1} or less. Contour interval of 4 m s^{-1} used for larger magnitudes. Rear-to-front flow is stippled.

"blocked" just inside the stratiform rain region (around $x = 48$ km).

The downward motion and adiabatic warming partially oppose the intense cooling from sublimation, melting, and evaporation. Potential temperature increases above the melting level in the region of subsidence where microphysical cooling is not pronounced (Fig. 7). Significant cooling generally occurs below this level, with some warming near the surface in the region of strongest descent and heaviest rainfall. By 60 min (Fig. 7a) θ has decreased during the simulation by around 4 K in the region of heaviest rainfall, and over 6 K around the 3.5-km level downwind of the heaviest rainfall. Warming of up to 2 K has occurred below the cooling at around the 1-km level. Warming aloft is as large as 2.4 K in the same general region. At 75 min,

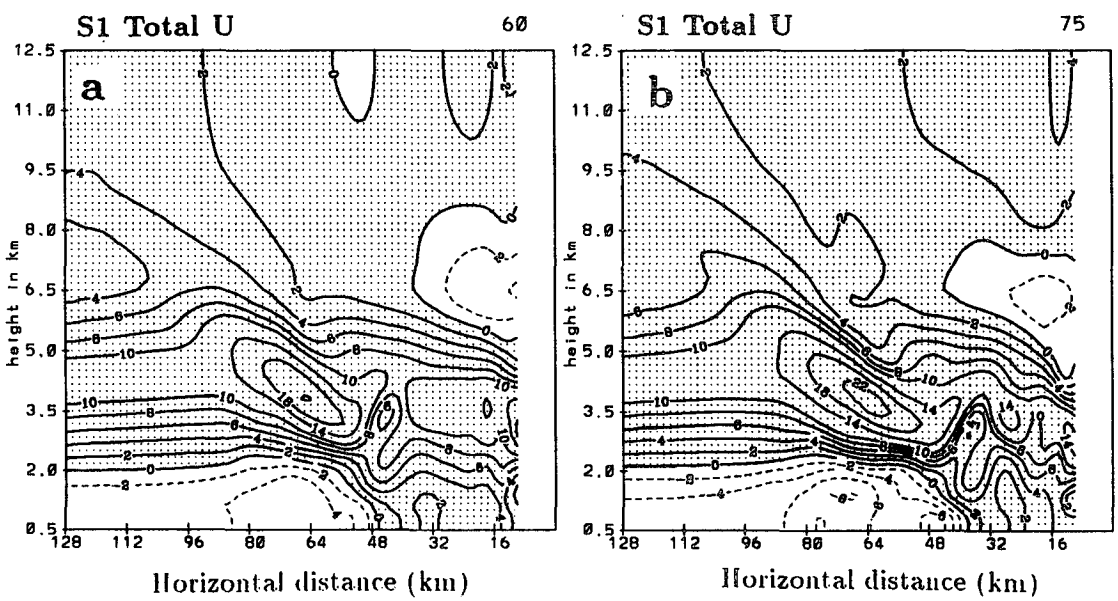

FIG. 6. Total u component of the wind (m s^{-1}) for S1 at (a) 60 and (b) 75 min.

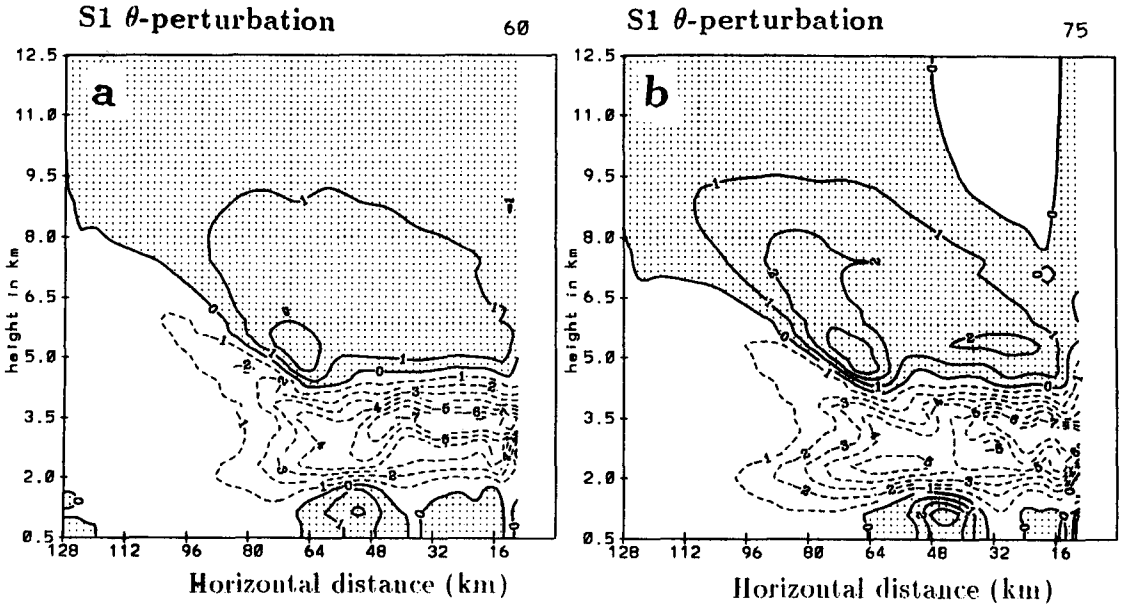

FIG. 7. Potential temperature change (K) since initial time at (a) 60 and (b) 75 min, with contour interval of 1 K. Warming is stippled.

the peak cool anomaly in the heaviest rainfall has increased to over 5 K, while up to 7.5-K cooling has taken place downwind of this region (Fig. 7b). The layer of strongest cooling in the heavy rain region has lowered, and this trend was persistent throughout the simulation. Warming at the surface at this time increases to over 3 K in an area where subsidence is strong close to the surface ($x \approx 45$ km). Warming aloft at the top of the main downdraft reaches over 3 K at this time.

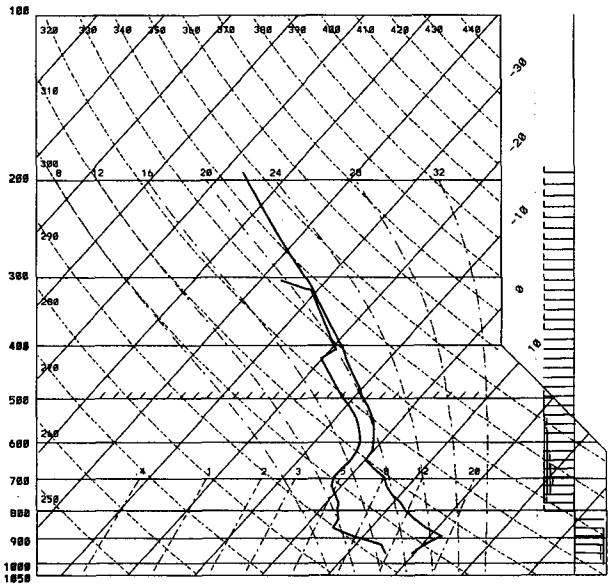

FIG. 8. Thermodynamic diagram taken from region with strong low-level warming ($x = 48$ km) at 75 min in simulation S1.

A sounding taken in this region of strong low-level warming at 75 min shows the changes that have taken place since the start of the simulation (Fig. 8). Significant cooling has occurred in the 600–850-mb layer, so that the lapse rate has become nearly dry adiabatic there. Substantial warming occurs below 850 mb, with the other region of warming showing up above the melting level. Drying has also taken place in the lowest 1–2 km, with substantial moistening above this level. The steep lapse rates above a low-level inversion, and dry air around the 850-mb level are typical of "onion" soundings often observed in the vicinity of the mesoscale downdraft in the stratiform region (Zipser 1977). A comparison of the potential temperature field between 60 and 75 min (Fig. 7) shows that substantial warming (generally over 1 K) does occur at the sounding site ($x = 46$ km) during this 15-min period at nearly all levels below 5 km. Observations, however, show that low-level warming and drying were more substantial near the wake low (Stumpf et al. 1991), with warming of 3–4 K in much of the atmosphere below 5 km during the 90-min period ending at 0130 UTC 4 June.

The temperature changes that occur in this simulation are significant and induce substantial pressure variations in the domain (Fig. 9). The hydrostatic pressure perturbations (change in hydrostatic pressure since initialization) in the domain at 60 min (Fig. 9a) indicate a low pressure area at midlevels in the region of heavy precipitation. At the surface, a weak pressure gradient exists with lower pressure behind the system. Highest

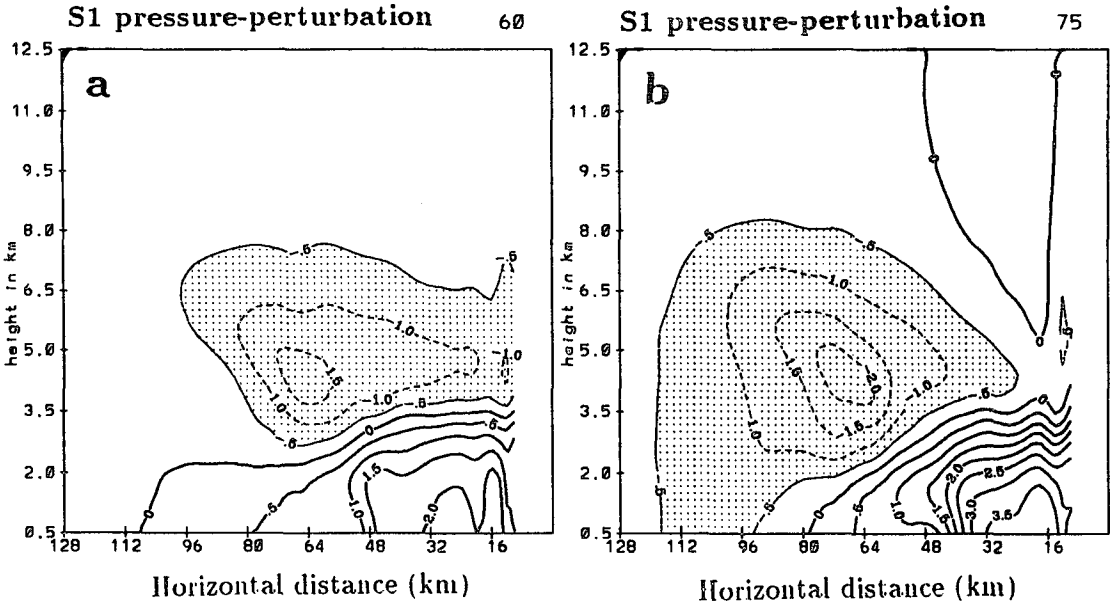

FIG. 9. Hydrostatically calculated pressure perturbation (pressure change since initial time in mb) in S1 at (a) 60 and (b) 75 min, with contour interval of 0.5 mb. Negative perturbations exceeding 0.5 mb are stippled.

pressures occur downwind of the heaviest surface rainfall. Surface pressures have not fallen during the simulation, but a tighter pressure gradient has developed just downwind of the heaviest surface rainfall (around $x = 48$ km).

At 75 min (Fig. 9b), perturbation pressure features strengthen significantly. The midlevel mesolow intensifies with a negative perturbation of nearly 2.5 mb. At the surface, relatively lower pressure continues to be found to the rear of the precipitation region with higher pressure in the rain region. Surface pressures have fallen by as much as 0.8 mb, at a distance of over 20 km rearward of the back edge of surface rainfall. The pressure gradient is rather weak, except within the primary rain region where a 2-mb gradient exists over a 10-km distance.

The wake low and the pressure gradient are much more intense than those found in the simulations of the 10–11 June system where the jet descended gradually (GJa). However, these features are not as strong or as widespread as observed on 4 June. Stumpf et al. (1991) found a pressure gradient as large as 2 mb over a 5-km distance around 0100 UTC 4 June, with a 1 mb (10 km)$^{-1}$ gradient occurring over a rather wide area (50–70 km). Stumpf et al. determined that 90% of the pressure changes were hydrostatically induced. The lowest pressure in the simulated wake low occurs in roughly the same position relative to the rain region as was observed, roughly 20 km behind the tight reflectivity gradient (Stumpf et al. 1991). The wake low and reflectivity field were similarly related in the 10–11 June system (Augustine and Zipser 1987; Smull and Houze 1987; Johnson and Hamilton 1988; Rutledge et al. 1988). The observed pressure gradient, however, in the 4 June system was tightest in the region of tightest reflectivity gradient. The model results do not agree with this observation (see Fig. 3). (Note that the gradient of the reflectivity field by definition coincides with the gradient of rainwater.)

Many sensitivity tests were run initialized with different soundings, and using different amounts of snow aloft. These simulations were unable to produce a wake low of stronger intensity or broader scale. In general, stronger descent, as large as 5 m s^{-1} in some simulations, requires heavier snowfall aloft and/or drier conditions near the melting level, which result in increased microphysical cooling that easily opposes adiabatic warming so that pressure falls at the surface are not increased. To reduce microphysical cooling requires less snow, or moister conditions that weaken the downdraft and the adiabatic warming. The model is unable to produce strong descent and warming from the effects of light precipitation. A balance exists between the cooling necessary to drive strong subsidence and the adiabatic warming produced by the descent.

Although this simulation produces a much stronger wake low at the surface than in the 10–11 June simulations discussed in GJa and GJb, by allowing hydrometeors to advect into drier air in an environment whose stability is already altered by the stratiform region, the wake low is still not as intense, and is more limited in its extent than observed on 4 June. As will be shown below, the underestimate of wake low intensity may be the result of the prescribed constant pre-

cipitation intensity (implying an expanding stratiform region).

4. Simulation with decreasing snow field

Simulations were also done with the 2-km horizontal mesh version of the model allowing precipitation rates to decrease significantly over time. These simulations can be thought of as representing systems where collapsing precipitation cores exist within the stratiform region, or a tight reflectivity gradient at the rear of the region advances rapidly with time. As stated in the introduction, such rapid decreases in stratiform region precipitation intensity have been observed (e.g., Johnson et al. 1989), but it is beyond the scope of this study, or the abilities of this simple model, to explore the causes for such behavior. Simulations of the 10–11 June case with this model (GJa, GJb) were driven by convective inputs, which were allowed to decrease substantially after a time, following the pattern of observations; however, significant production of condensate within a well-developed mesoscale updraft prevented the decrease from affecting hydrometeor fields toward the rear of the stratiform region. Interaction of the MCS circulation with the larger-scale flow field may contribute to more rapid variations in precipitation intensity in this portion of the stratiform region.

The decreasing precipitation rates in this simulation are produced by prescribing an initial snow field that decreases starting at 20 min to only 20% of its initial magnitude by 40 min. Although the decrease in the snow field in this simulation is done across the domain, results are generally similar to a sensitivity test in which only the rearmost 40 km of the snow field experienced the decrease. These simulations generally produced similar features to S1, but with more intense warming, and a more pronounced wake low that better agreed with observations. One simulation, S2, will be discussed in detail below.

Snow again is the only hydrometeor present initially in S2, and the snow field is the same as that used in S1 (Fig. 2). After the snow contents decrease rapidly between 20 and 40 min, the mixing ratios are then maintained at this smaller level throughout the rest of the simulation. The snow field at 75 min (during this period when prescribed rates are held constant at the reduced value) is shown in Fig. 10. The evolution of the snow field causes the heaviest rainfall to occur at around 45 min near $x = 64$ km (Fig. 11a) in S2. Peak surface rain rates are around 6 mm h^{-1}, or rather similar to those at 60 min in S1, and generally typical of heavier observed stratiform region rainfall (Johnson and Hamilton 1988; Gallus and Johnson 1991). By 60 min (Fig. 11b) rain rates decrease significantly with peak surface values barely over 1 mm h^{-1}. Rainfall continues to decrease through 75 min when all values are less than 1 mm h^{-1} at the surface (Fig. 11c). This decrease of over 5 mm h^{-1} in rain intensity over 30

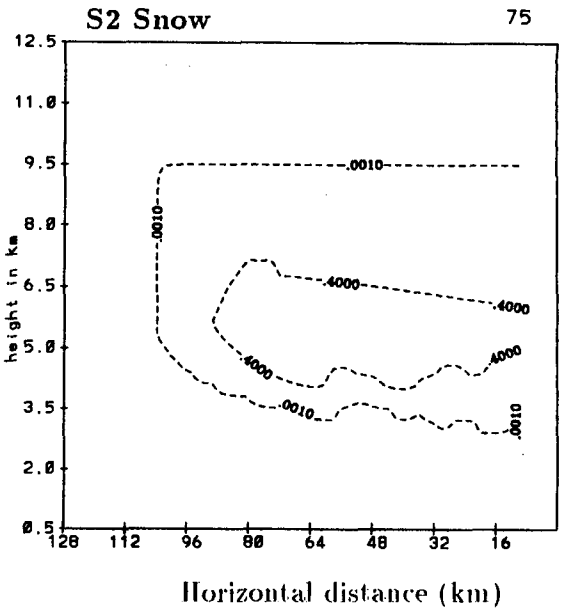

FIG. 10. Snow mixing ratio at 75 min for S2, the simulation in which the snow field decreases with time.

min is supported by observations at some mesonet sites on 4 June (Stumpf et al. 1991).

The initially heavy precipitation induces a strong downdraft that is most intense around 60 min (Fig. 12a). Peak descent occurs just in front of the heaviest rainfall and is around 1.4 m s^{-1}, or 20% less than the peak descent in S1, which occurred at 75 min. The downdraft weakens slightly in S2 at 75 min (Fig. 12b) with peak descent of 1.0 m s^{-1} at that time. The strongest descent in S2 occurs below 3 km, as the higher level maxima in descent present in S1 has weakened markedly. Horizontal velocity perturbations in S2 (Fig. 13) are similar to those in S1, although peak RTF flow is approximately 30% smaller by 75 min (Fig. 13b). In addition, FTR flow near the surface is somewhat stronger in S2 at around $x = 48$ km at 75 min. As will be shown later, this increase in FTR flow is related to a more intense wake low in this region. The total flow field in S2 is again similar to that in S1, with the only significant differences being a slight weakening of the peak RTF flow at around the 4-km level, and a slight increase in low-level FTR flow near $x = 48$ km (figure not shown).

The downward motion and adiabatic warming are again opposed significantly by evaporative cooling, but low-level warming is increased in S2 (Fig. 14) from that in S1 (Fig. 7). Peak cooling near the melting level is only about 1 K less than in S1. Warming above the melting level is not as strong in S2 as in S1. A rather significant decrease in the cooling in the 2–5-km layer occurs in the region of strongest descent in S2 compared with S1, especially at 75 min (Fig. 14b).

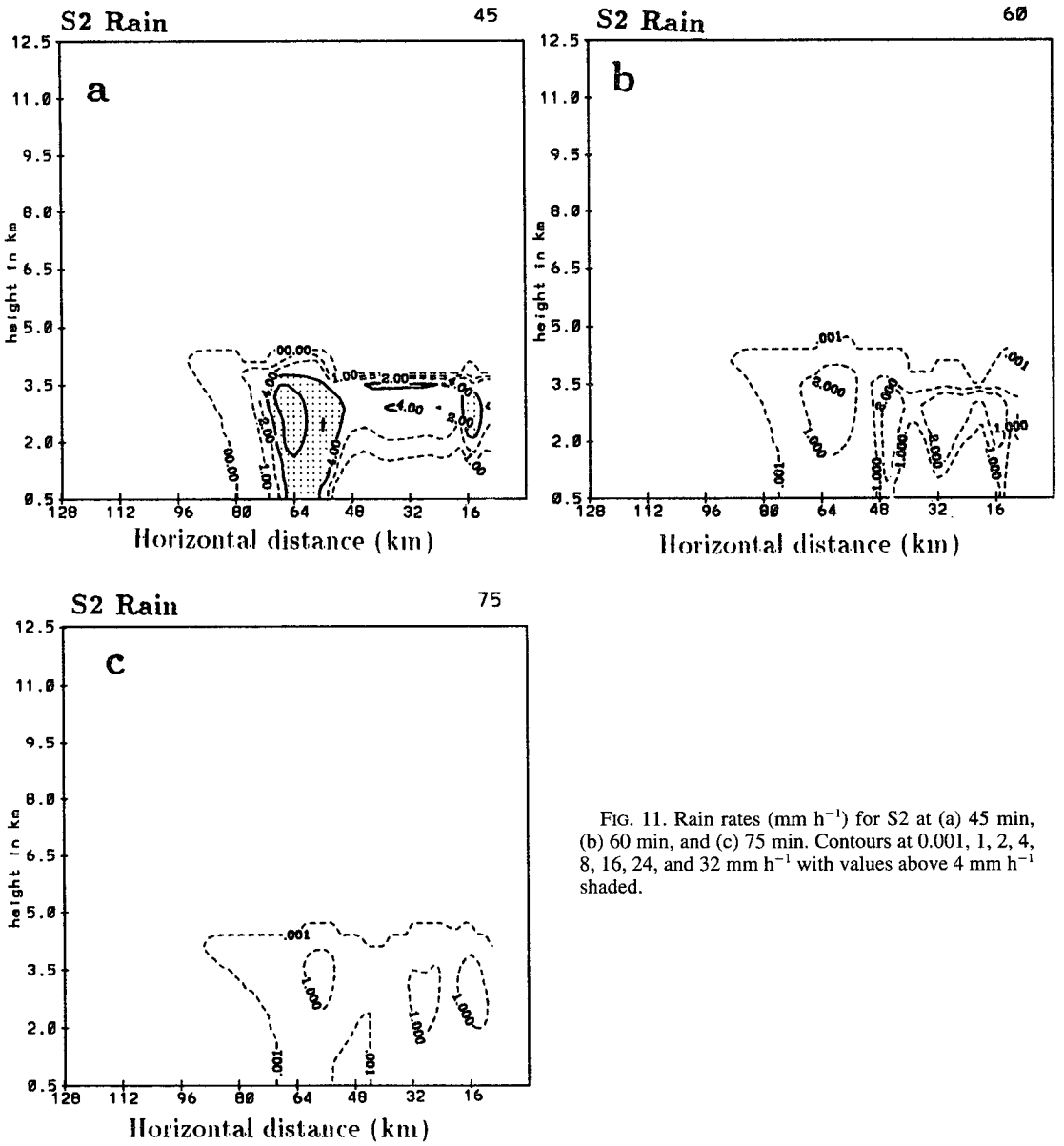

FIG. 11. Rain rates (mm h^{-1}) for S2 at (a) 45 min, (b) 60 min, and (c) 75 min. Contours at 0.001, 1, 2, 4, 8, 16, 24, and 32 mm h^{-1} with values above 4 mm h^{-1} shaded.

Whereas cooling greater than 4 K occurred at at least one level for all points within the rain region of S1, a small region in S2 experiences no more than 3-K cooling at any level. The greatly reduced rain rates in S2 result in less microphysical cooling to oppose adiabatic warming. Low-level warming in S2 is approximately 1.5 K greater by 75 min (Fig. 14b) than in S1.

A sounding taken in this region of greatest low-level warming (Fig. 15) is substantially warmer at all levels below 600 mb than the sounding shown from simulation S1 (Fig. 8). It is also significantly drier from 550 to 850 mb than the S1 sounding. The increased warming and drying at low levels results in a sounding that more closely agrees with those observed near the wake low of this case (Stumpf et al. 1991). It should be noted, however, that although the warming and drying that have occurred during the simulation are greater than in S1 at low levels, cooling and moistening have still occurred since the initial time closer to the melting level. Stumpf et al. (1991) show that warming and drying occurred over a deep layer in Russell, Kansas, extending from nearly the surface to 500 mb between 0000 and 0130 UTC on 4 June, during the period that the wake low greatly intensified. The low-level reflectivity field covered Russell much of this time, implying that some microphysical cooling would have been occurring. A comparison of the model potential temperature perturbation fields at 60 and 75 min (Fig. 14)

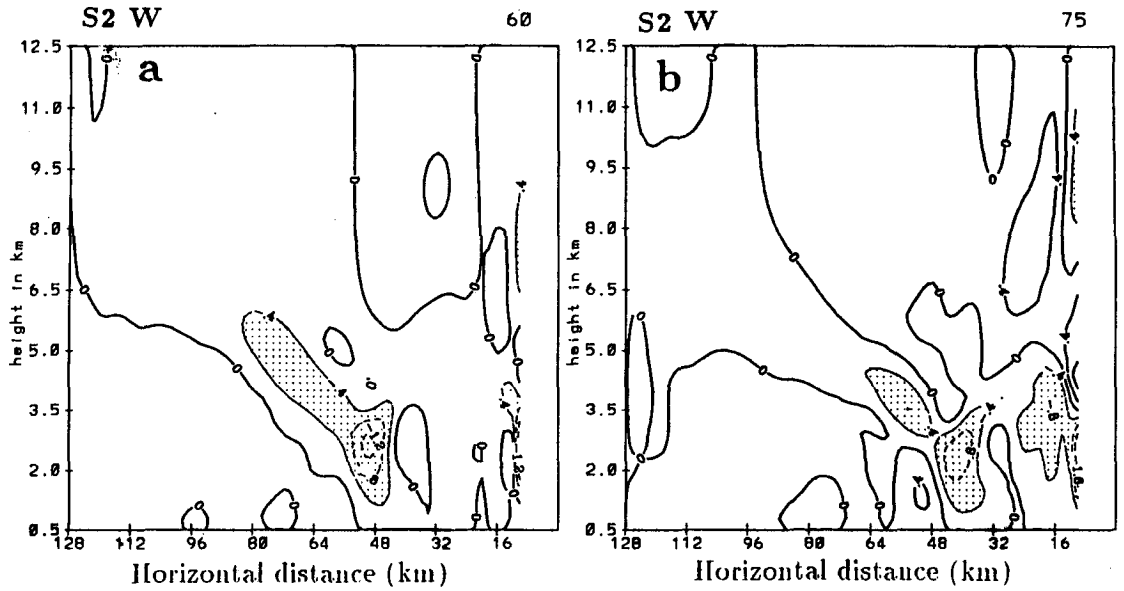

FIG. 12. Vertical velocity (m s^{-1}) for S2 at (a) 60 and (b) 75 min, with contour interval of 0.4 m s^{-1}. Values of descent larger than 0.4 m s^{-1} are shaded.

shows that warming does occur over a deep layer during this 15-min period near $x = 46$ km. In fact, as much as 3–4 K of warming has occurred around the 3.5-km level, in close agreement with that observed during the 0000–0130 UTC time frame at Russell (Stumpf et al. 1991). In the model, warming and drying do not occur until after 60 min when precipitation becomes negligible. Cooling was substantial prior to that time, even with modest rainfall rates. This suggests that either another mechanism not able to be reproduced in this simple model was forcing higher and/or stronger descent better able to overcome microphysical cooling in the 4 June case, or that significant warming and drying must occur quickly when precipitation becomes negligible. Much of the warming that occurred in the Russell sounding between 0000 and 0130 UTC may have taken

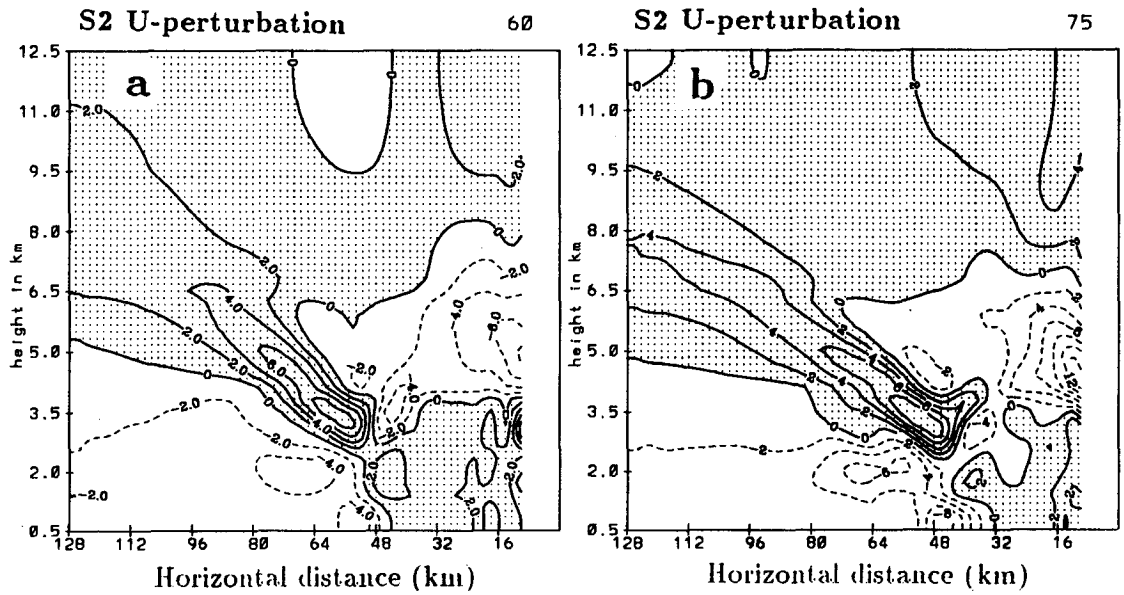

FIG. 13. U-perturbation velocities (m s^{-1}) for S2 at (a) 60 and (b) 75 min, with contour interval of 2 m s^{-1} for magnitudes of 10 m s^{-1} or less. Contour interval of 4 m s^{-1} used for larger magnitudes. Rear-to-front flow is stippled.

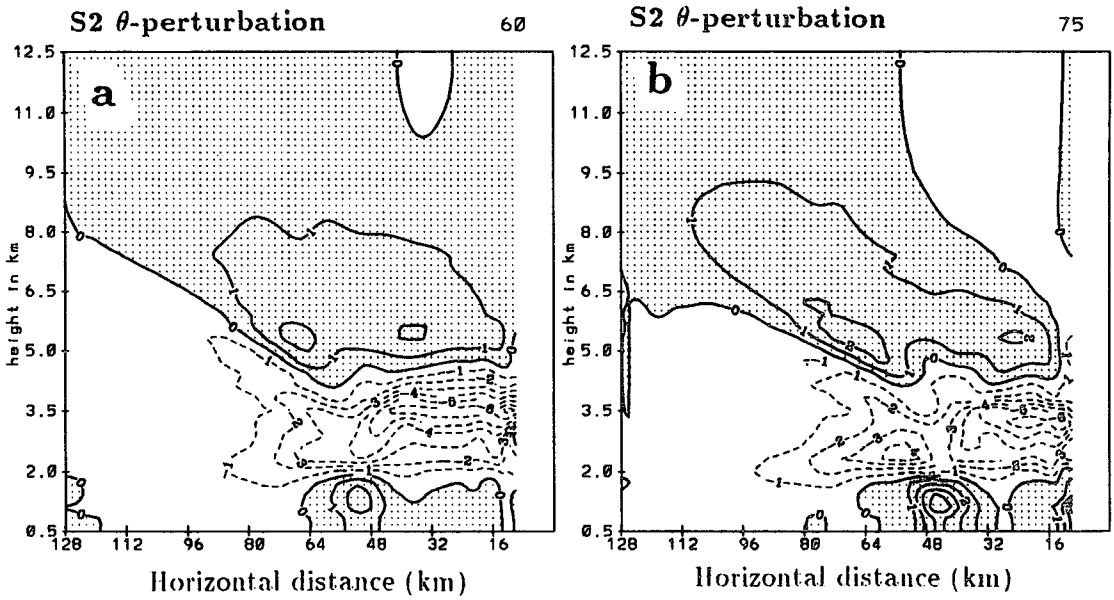

FIG. 14. Potential temperature change (K) since initial time at (a) 60 and (b) 75 min, with contour interval of 1 K. Warming is stippled.

place within only a small portion of the 90 min, after the heavier reflectivities had moved east.

The warming that occurs in S2 results in a hydrostatically induced wake low (Fig. 16) that is deeper relative to nearby regions than in S1 (Fig. 9). More importantly, the wake low develops more quickly and closer to the tight pressure gradient. At 60 min (Fig. 16a) the relative pressure minimum first develops at x = 54 km with a perturbation of over 1.0 mb. A pressure gradient of roughly 1.5 mb exists over a 10-km distance immediately ahead of the low. By 75 min, pressures have fallen behind the main rain area, and are nearly 1 mb lower than in S1. Pressures at x = 46 km have fallen 1 mb in the preceding 15 min, and a secondary maximum in wake low strength occurs here. The gradient of pressure here is about 2 mb over 10 km, or similar to that in S1. The primary difference is that the tight pressure gradient occurs just ahead of the wake low, in better agreement with observations of the 4 June case (Stumpf et al. 1991). The wake low weakens slightly at 90 min (figure not shown) but is still rather pronounced. The large pressure falls at 75 min are occurring with descent that is nearly 50% smaller than in S1. With significantly reduced evaporative cooling, the adiabatic warming is able to induce a stronger wake low.

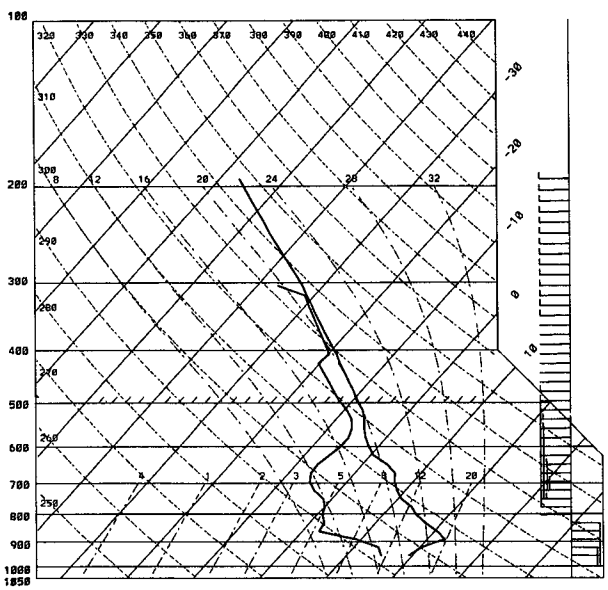

FIG. 15. Thermodynamic diagram taken from region with strong low-level warming (x = 48 km) at 75 min in simulation S2.

Simulation S2 implies that temporal or spatial variations in the precipitation intensity may be crucial in the development of an intense wake low. Although descent is stronger in S1 than in S2, the heavy rainfall occurring over a long time period does not permit adiabatic warming to oppose the microphysical cooling sufficiently to reduce pressures markedly from those in other portions of the domain. Collapsing precipitation cores, or rapid decreases in precipitation intensity at a fixed location, as represented in simulation S2, appear to induce fairly strong descent that continues even after the precipitation rates have become very light. Because descent as large as 1 m s^{-1} continues in the presence of rain rates less than 1–2 mm h^{-1}, adiabatic warming is not as strongly opposed by microphysical cooling, and pressures can drop much more in a small region

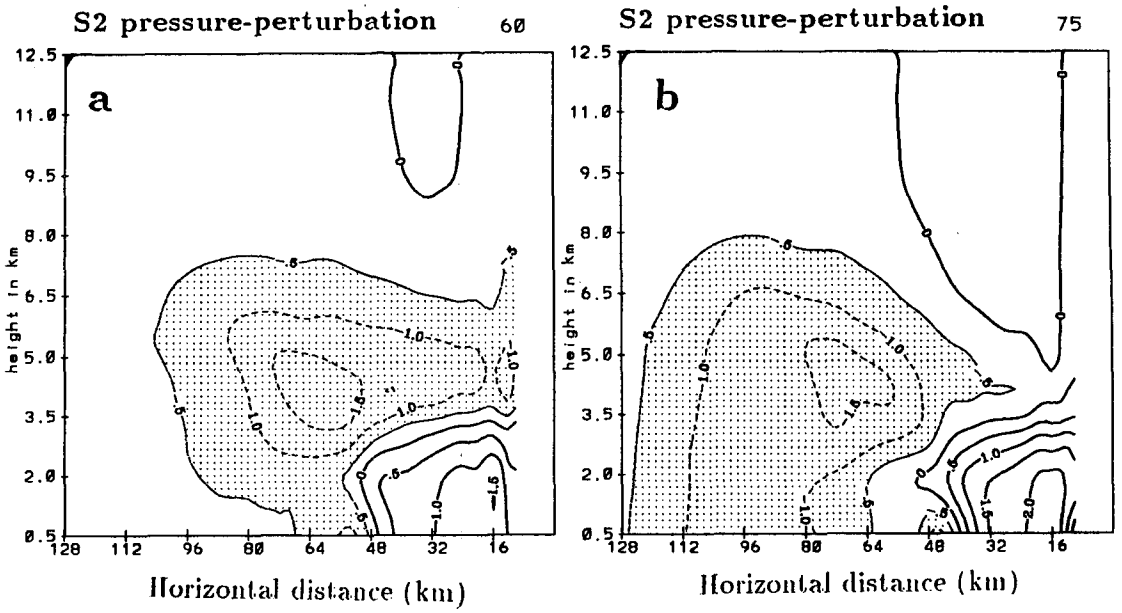

FIG. 16. Hydrostatically calculated pressure perturbation (mb, pressure change since initial time) in S2 at (a) 60 and (b) 75 min, with contour interval of 0.5 mb. Negative perturbations exceeding 0.5 mb are stippled.

than in nearby areas. This result agrees well with observations and is consistent with the hypothesis for wake lows advanced by Johnson and Hamilton (1988).

5. Conclusions and discussion

A two-dimensional cloud model, developed using the bulk microphysical parameterization of the kinematic Rutledge and Hobbs (1983; 1984) model, is used to determine whether microphysical processes alone can explain the sudden descent of rear-inflow jets and the formation of intense surface wake lows in some MCSs. The domain is applied to a portion of the stratiform region capturing the back edge of the surface rain area. Significant amounts of snow falling into a rear-inflow jet induce strong descent exceeding 1.5 m s^{-1}. However, the microphysical cooling from sublimation, melting, and evaporation strongly opposes adiabatic warming so that pressure falls at the surface are modest in a simulation representing an expanding stratiform region. The intensity of the surface wake low is similar in sensitivity tests where the intensity of the precipitation is varied.

In a simulation representing either a collapsing precipitation core, or rapidly moving tight reflectivity gradient at the back of a stratiform region, strong descent develops in the same region at the back of the stratiform area, but it is weaker than in a simulation with constant or increasing precipitation rates. However, the rapidly diminishing precipitation results in less microphysical cooling, so that the adiabatic warming can cause larger pressure falls at the surface with a wake low accompanied by an intense pressure gradient. The pressure field in this simulation is in better agreement with the observed field in the 3–4 June PRE-STORM case.

This study suggests that a vertical circulation must persist after the microphysical forcing is reduced in order for a strong wake low to form. After the perturbation potential energy source is reduced, buoyancy forces begin to increasingly oppose the vertical circulation in a stable atmosphere, and perturbation kinetic energy is transformed into perturbation potential energy. If the weakened downdraft lags the reduced microphysical cooling by just enough, a strong wake low can form before increasing positive buoyancy forcing begins to retard and eventually reverse the circulation. The wake low induced from microphysical forcing alone must therefore be a transient phenomenon.

The simulations do not exclude the possibility that some other dynamic effect not able to be simulated with this simple model plays a role in cases of strong subsidence and intense surface pressure falls. If subsidence related to gravity wave circulations (Schmidt and Cotton 1990) occurs rearward of the main region of microphysical cooling, warming should be pronounced with significant surface pressure falls. Interactions between existing jets or possible blocking mechanisms that might enhance subsidence and adiabatic warming are not simulated fully with this model, at least partly because of its horizontally homogeneous initialization of flow. However, the fact that strong subsidence and an intense wake low are simulated even with the limitations of the 2D model implies that microphysical

cooling may indeed be the only mechanism necessary to produce these features.

Acknowledgments. The author would like to thank Prof. Richard Johnson for his helpful comments and support during this research. The constructive comments of two anonymous reviewers significantly improved the paper. This research has been supported by a National Science Foundation Graduate Fellowship and National Science Foundation Grant ATM9013112. Final preparation of the manuscript was permitted under the UCAR visiting scientist program at the National Meteorological Center.

REFERENCES

Augustine, J. A., and E. J. Zipser, 1987: The use of wind profilers in a mesoscale experiment. *Bull. Amer. Meteor. Soc.*, **68,** 4–17.

Bernstein, B. C., and R. H. Johnson, 1994: A dual-Doppler radar study of an OK PRE-STORM heat burst event. *Mon. Wea. Rev.*, **122,** 259–273.

Bosart, L. F., and A. Seimon, 1988: A case study of an unusually intense atmospheric gravity wave. *Mon. Wea. Rev.*, **116,** 1857–1886.

Braun, S. A., and R. A. Houze Jr., 1995: Melting and freezing in a mesoscale convective system. *Quart. J. Roy. Meteor. Soc.*, **121,** 55–77.

Caniaux, G., J.-P. Lafore, and J.-L. Redelsperger, 1995: A numerical study of the stratiform region of a fast-moving squall line. Part II: Relationship between mass, pressure, and momentum fields. *J. Atmos. Sci.*, **52,** 331–352.

Fovell, R. G., and Y. Ogura, 1989: Effect of vertical wind shear on numerically simulated multicell storm structure. *J. Atmos. Sci.*, **46,** 3144–3176.

Gallus, W. A., Jr., and R. H. Johnson, 1991: Heat and moisture budgets of an intense midlatitude squall line. *J. Atmos. Sci.*, **48,** 122–146.

——, and ——, 1995a: The dynamics of circulations within the trailing stratiform regions of squall lines. Part I: The 10–11 June PRE-STORM system. *J. Atmos. Sci.*, **52,** 2161–2187.

——, and ——, 1995b: The dynamics of circulations within the trailing stratiform regions of squall lines. Part II: Influence of the convective line and ambient environment. *J. Atmos. Sci.*, **52,** 2188–2211.

Johnson, R. H., and P. J. Hamilton, 1988: The relationship of surface pressure features to the precipitation and air flow structure of an intense midlatitude squall line. *Mon. Wea. Rev.*, **116,** 1444–1472.

——, and D. L. Bartels, 1992: Circulations associated with a mature-to-decaying midlatitude mesoscale convective system. Part II: Upper-level features. *Mon. Wea. Rev.*, **120,** 1301–1320.

——, S. Chen, and J. J. Toth, 1989: Circulations associated with a mature-to-decaying midlatitude mesoscale convective system. Part I: Surface features—Heat bursts and mesolow development. *Mon. Wea. Rev.*, **117,** 942–959.

Lafore, J.-P., and M. W. Moncrieff, 1989: A numerical investigation of the organization and interaction of the convective and stratiform regions of tropical squall lines. *J. Atmos. Sci.*, **46,** 521–524.

Leary, C. A., and R. A. Houze Jr., 1979: Melting and evaporation of hydrometeors in precipitation from the anvil clouds of deep tropical convection. *J. Atmos. Sci.*, **36,** 669–679.

Lin, Y.-L., R. D. Farley, and H. D. Orville, 1983: Bulk parameterization of the snow field in a cloud model. *J. Climate Appl. Meteor.*, **22,** 1065–1092.

Miller, M. J., and A. K. Betts, 1977: Traveling convective storms over Venezuela. *Mon. Wea. Rev.*, **105,** 833–848.

Nicholls, M. E., 1987: A comparison of the results of a two-dimensional numerical simulation of a tropical squall line with observations. *Mon. Wea. Rev.*, **115,** 3055–3077.

——, and M. J. Weissbluth, 1988: A comparison of two-dimensional and quasi-three-dimensional simulations of a tropical squall line. *Mon. Wea. Rev.*, **116,** 2437–2452.

Ogura, Y., and N. A. Phillips, 1962: Scale analysis of deep and shallow convection in the atmosphere. *J. Atmos. Sci.*, **19,** 173–179.

Rutledge, S. A., 1986: A diagnostic numerical study of the stratiform region associated with a tropical squall line. *J. Atmos. Sci.*, **43,** 1337–1358.

——, and P. V. Hobbs, 1983: The mesoscale and microscale structure and organization of clouds and precipitation in midlatitude cyclones. VIII: A model for the "seeder–feeder" process in warm-frontal rainbands. *J. Atmos. Sci.*, **40,** 1185–1206.

——, and ——, 1984: The mesoscale and microscale structure and organization of clouds and precipitation in midlatitude cyclones. XII: A diagnostic modeling study of the precipitation development in narrow cold-frontal rainbands. *J. Atmos. Sci.*, **41,** 2949–2972.

——, and R. A. Houze Jr., 1987: A diagnostic modeling study of the trailing stratiform region of a midlatitude squall line. *J. Atmos. Sci.*, **44,** 2640–2656.

——, ——, M. I. Biggerstaff, and T. Matejka, 1988: The Oklahoma–Kansas mesoscale convective system of 10–11 June 1985: Precipitation structure and single-Doppler radar analysis. *Mon. Wea. Rev.*, **116,** 1409–1430.

Schmidt, J. M., and W. R. Cotton, 1990: Interactions between upper and lower tropospheric gravity waves on squall line structure and maintenance. *J. Atmos. Sci.*, **47,** 1205–1222.

Scott, J. D., and S. R. Rutledge, 1995: Doppler radar observations of an asymmetric mesoscale convective system and associated vortex couplet. *Mon. Wea. Rev.*, **123,** 3437–3457.

Smull, B. F., and R. A. Houze Jr., 1987: Rear inflow in squall lines with trailing stratiform precipitation. *Mon. Wea. Rev.*, **115,** 2869–2889.

Stensrud, D. J., R. A. Maddox, and C. L. Ziegler, 1991: A sublimation-initiated mesoscale downdraft and its relation to the wind field below a precipitating anvil cloud. *Mon. Wea. Rev.*, **119,** 2124–2139.

Stumpf, G. J., R. H. Johnson, and B. F. Smull, 1991: The wake low in a midlatitude mesoscale convective system having complex convective organization. *Mon. Wea. Rev.*, **119,** 134–158.

Szeto, K. K., R. E. Stewart, and C. A. Lin, 1988: Mesoscale circulations forced by melting snow. Part II: Application to meteorological features. *J. Atmos. Sci.*, **45,** 1642–1650.

Thorpe, A. J., M. J. Miller, and M. W. Moncrieff, 1980: Dynamical models of two-dimensional downdraughts. *Quart. J. Roy. Meteor. Soc.*, **106,** 463–484.

Williams, D. T., 1954: A surface study of a depression-type pressure wave. *Mon. Wea. Rev.*, **82,** 289–295.

——, 1963: The thunderstorm wake of 4 May, 1961. Natl. Severe Storms Project Rep. 18, U.S. Department of Commerce, Washington, DC, 23 pp. [NTIS PB 168223.]

Willis, P. T., and A. J. Heymsfield, 1989: Structure of the melting layer in mesoscale convective system stratiform precipitation. *J. Atmos. Sci.*, **46,** 2008–2025.

Zhang, D.-L., and K. Gao, 1989: Numerical simulations of an intense squall line during 10–11 June 1985 PRE-STORM. Part II: Rear inflow, surface pressure perturbations and stratiform precipitation. *Mon. Wea. Rev.*, **117,** 2067–2094.

——, ——, and D. B. Parsons, 1989: Numerical simulation of an intense squall line during 10–11 June 1985 PRE-STORM. Part I: Model verification. *Mon. Wea. Rev.*, **117,** 960–994.

Ziegler, C. L., 1985: Retrieval of thermal and microphysical variables in observed convective storms. Part I: Model development and preliminary testing. *J. Atmos. Sci.*, **42,** 1487–1509.

Zipser, E. J., 1977: Mesoscale and convective-scale downdrafts as distinct components of squall-line circulations. *Mon. Wea. Rev.*, **105,** 1568–1589.